Crystal structure of the p27^{Kip1} cyclin-dependent-kinase inhibitor bound to the cyclin A–Cdk2 complex

Alicia A. Russo, Philip D. Jeffrey, Andrea K. Patten, Joan Massagué* & Nikola P. Pavletich

Cellular Biochemistry and Biophysics Program, * Cell Biology Program and the Howard Hughes Medical Institute, Memorial Sloan-Kettering Cancer Center, New York, New York 10021, USA

The crystal structure of the human p27^{Kip1} kinase inhibitory domain bound to the phosphorylated cyclin A–cyclin-dependent kinase 2 (Cdk2) complex has been determined at 2.3 Å. p27^{Kip1} binds the complex as an extended structure interacting with both cyclin A and Cdk2. On cyclin A, it binds in a groove formed by conserved cyclin box residues. On Cdk2, it binds and rearranges the amino-terminal lobe and also inserts into the catalytic cleft, mimicking ATP.

COMPLEXES of cyclins with cyclin-dependent kinases (CDKs) play a central role in the control of the eukaryotic cell cycle[1]. The discovery of proteins that bind to and inhibit the catalytic activity of cyclin–CDK complexes has identified kinase inhibition as an intrinsic component of cell-cycle control (reviewed in refs 1–3). These inhibitors (CKIs) induce cell-cycle arrest in response to anti-proliferative signals, including contact inhibition and serum deprivation[4], TGF-β (ref. 5), myogenic[6], myeloid[7] and neuronal differentiation[8], and DNA-damage checkpoints[9]. The inhibitors, which are present in proliferating cells as well, may also help to coordinate cell-cycle progression by their redistribution between different cyclin–CDK complexes[10,11].

The inhibitors that have been identified so far can be grouped, according to sequence and functional similarities, into two families. The Kip/Cip family of inhibitors, which include p27^{Kip1} (refs 4, 12), p21$^{Cip1,WAF-1}$ (refs 9, 13–15) and p57^{Kip2} (refs 16, 17), bind to and inhibit cyclin–CDK complexes with broad preference for the G1 and S phase kinase complexes over the mitotic ones. The Kip/Cip inhibitors can bind isolated cyclin and CDK subunits independently, but they have a higher affinity for the cyclin–CDK complexes[12,18–20]. The INK4 family members, which include p15, p16, p18 and p19, are specific for Cdk4, and its close isoform Cdk6, and can bind to either the isolated CDK subunit or its complex with cyclin D[3].

Members of the Kip/Cip family contain a 65-amino-acid region with homology (38–44% identity) at their N-terminal portions, which is necessary and sufficient to bind to and inhibit cyclin–CDK complexes[4,16,18,21]. Their carboxy-terminal portions are variable in length and divergent in sequence and function[3].

Here we report the crystal structure of the 69-amino-acid N-terminal inhibitory domain of p27^{Kip1} bound to the phosphorylated cyclin A–Cdk2 complex, determined at 2.3 Å resolution (Table 1 and Fig. 1). The structure reveals that p27 uses a three-stage approach to bind and inhibit the cyclin A–Cdk2 complex. It binds a peptide-binding groove on the conserved cyclin box of cyclin A, it binds the N-terminal lobe of Cdk2 and it also inserts deep inside the catalytic cleft, mimicking ATP. A comparison of Cdk2 in this complex with the structure of Cdk2 in the binary cyclin A–Cdk2 complex[22,23] reveals that p27 binding causes large conformational changes in and around the catalytic cleft of Cdk2.

Overall structure of the complex

In the complex (Fig. 2*a*), the p27 inhibitory domain has a non-globular, extended structure that consists sequentially of a rigid coil, an amphipathic α-helix, an amphipathic β-hairpin, a β-strand and a 3_{10} helix (Fig. 2*b*). p27 does not have a hydrophobic core of its own, and its secondary structure elements do not interact significantly with each other.

The extended structure of p27 allows it to cover and interact with a large surface area of the cyclin A–Cdk2 complex. The surface area buried when p27 binds to the cyclin A–Cdk2 complex is 5,752 Å^2 (40% on cyclin A, 60% on Cdk2), which is significantly larger than other protein–protein complexes, including the cyclin A–Cdk2 complex (3,550 Å^2; ref. 22). The majority of the p27 hydrophobic amino acids pack against the cyclin A–Cdk2 complex (Fig. 2*b*) instead of participating in the folding of p27. The extended p27 structure can thus be thought of as refolding on the cyclin A–Cdk2 complex. This hypothesis is consistent with the large buried surface area per amino acid, which is comparable to that expected from protein folding[24].

The structure of the cyclin A subunit consists of two five-helix structural repeats, the first of which corresponds to the conserved cyclin box[22]. It is only the cyclin-box repeat that is involved in p27 binding (Fig. 2*a*), interacting with the rigid coil and α-helix of p27. The Cdk2 structure consists of an N-terminal lobe that is rich in β-sheet, and a larger, C-terminal lobe that is mostly α-helical, with the catalytic cleft in between the two lobes[22]. In the complex, the N-terminal lobe and catalytic cleft of Cdk2 bind the β-hairpin, β-strand, and 3_{10} helix of p27 (Fig. 2*a*).

The rigid coil of p27, which is 10-amino-acids long (Fig. 2*b*) and includes the sequence Leu-Phe-Gly conserved among all Kip/Cip family members (henceforth, the 'LFG' motif), binds a shallow groove on cyclin A in a partially extended conformation. This peptide-binding groove is formed by the α1, α3 and α4 helices of the cyclin-box repeat and is lined with amino acids highly conserved among members of the cyclin family (Fig. 2*a*; ref. 22). This may explain, in part, the ability of p27 to bind many of the cyclin–CDK complexes. The peptide-binding groove of cyclin A revealed by the structure is likely to be the docking site of tight binding substrates, such as p107, which also contain the LFG sequence motif[25]. Immediately after the LFG coil, the hydrophobic face of the amphipathic p27 helix packs against a surface formed by the α4 and α5 helices of the cyclin box. The interactions made by the helix are not as extensive as those made by the LFG coil, and we presume that they contribute less to the binding. The helix axis is directed towards Cdk2, and as the helix leaves the cyclin A area and encounters a gap on the surface of cyclin A–Cdk2 it becomes kinked and partially disordered (residues 49–53).

As the helix reaches Cdk2, it becomes well ordered again. The helix is followed by an amphipathic β-hairpin (Fig. 2*a*, *b*) whose hydrophobic face packs against the N-terminal β-sheet of Cdk2 (strands 3, 4 and 5), in a β-sandwich arrangement. Immediately

after the β-hairpin, a p27 β-strand displaces one from Cdk2 and is incorporated into the Cdk2 β-sheet (Fig. 2). The p27 3_{10} helix that follows, inserts into the catalytic cleft of Cdk2 (Fig. 2). The 3_{10} helix contains the Phe-Tyr pair of amino acids which become buried deep inside the catalytic cleft, and which mimic the purine base of the ATP in their van der Waals and hydrogen bond contacts to Cdk2.

Binding of p27 to Cdk2 is accompanied by extensive structural changes in the N-terminal lobe and catalytic cleft of Cdk2. The Cdk2 β-sheet flattens and presents hydrophobic side chains to p27. In the binary complex, these side chains interact with each other instead, owing to the large curvature of the β-sheet. A strand of the Cdk2 β-sheet is replaced with one from p27, and this moves another Cdk2 strand by as much as 8.5 Å. These changes, together with the bulky 3_{10} helix binding, widen the catalytic cleft.

Inhibition of kinase activity by p27 thus has several components.

TABLE 1 Statistics from the crystallographic analysis

Data set	Native	$HgCl_2$	Thimerosal	Uranyl acetate
Resolution (Å)	2.3	2.8	3.0	3.2
Observations	162339	124684	65378	21031
Unique reflections	34683	17569	15964	10528
Data coverage (%)	96.1	86.1	96.0	77.0
R_{sym} (%)	5.6	7.2	7.3	9.1
MIR analysis (20.0–3.2 Å):				
Mean isomorphous difference		0.18	0.29	0.17
Phasing power		1.4	0.9	0.7
Refinement:				
Resolution range (Å)	7.0–2.3			
R-factor	19.2			
Reflections with $\|F\| > 2\sigma$	31351			
Number of atoms	5181			
Number of waters	197			
R.m.s.* bond lengths (Å)	0.012			
R.m.s.* bond angles (deg)	1.45			
R.m.s.* B-factors (Å^2)	3.26			

Preparation of ternary complex. The structural organization of the p27 protein[4] was characterized using subtilisin digestion which yielded an N-terminal fragment (residues 28–96) that contained CDK-inhibitory activity essentially identical to that of full-length p27, and a C-terminal fragment (residues 123–198). Recombinant human p27 inhibitory domain, corresponding to residues 22–106, was overexpressed in *Escherichia coli* using the pET3a vector (Novagen) according to standard procedures. The soluble fraction of the *E. coli* lysate was clarified over a Q-Sepharose column, the flow-through of which was applied to a heparin sulphate column at pH 6.0. The p27 fragment was eluted with a NaCl gradient, concentrated by ultrafiltration, and further purified by gel-filtration chromatography. Differential scanning calorimetry (data not shown) showed that the isolated p27 domain was not folded, suggesting that it may need the C-terminal domain to remain folded. Alternatively, the isolated inhibitory domain may be in partly folded states that are resistant to digestion, but which do not represent a single state that can be detected calorimetrically. To prepare the p27–cyclin A–Cdk2 complex, a twofold molar excess of the recombinant inhibitory domain was mixed with the phosphorylated cyclin A–Cdk2 complex, prepared as described[23], at a total protein concentration of 13 mg ml^{-1} (determined by ultraviolet absorption at 280 nm, calibrated using standard extinction coefficients for Phe, Tyr and Trp amino acids). The mixture was fractionated by gel-filtration chromatography, yielding a peak at a retention volume corresponding to a relative molecular mass of 70K containing the ternary complex at an ~1:1:1 molar ratio, and a second peak containing a onefold molar excess of free p27. The ternary complex peak has H1 histone kinase activity about 1% that of the phosphorylated binary complex[23] when assayed at a concentration of 10 nM, which is about an order of magnitude above the K_i of p27 for the related cyclin E–Cdk2 complex[20]. The residual activity probably results from the destabilization of the complex owing to its low concentration, because the residual activity can be made arbitrarily small by performing the kinase assay at concentrations well above the K_i (data not shown). The ternary complex peak was concentrated by ultrafiltration to 30 mg ml^{-1} in a buffer of 40 mM HEPES, 200 mM NaCl and 5 mM dithiothreitol, pH 7.0. **Crystallization and data collection.** Crystals were grown at 4 °C by the hanging-drop vapour-diffusion method, by mixing the complex with an equal volume of the well buffer containing 35% saturated ammonium sulphate, 40 mM HEPES, 5 mM dithiothreitol, pH 7.0. The crystals form in space group $P2_12_12_1$ with $a = 73.8$, $b = 78.3$, $c = 137.2$ Å and contain one complex in the asymmetric unit. Diffraction data were collected at −170 °C (ref. 22) using an R-AXISIIC imaging plate detector mounted on a Rigaku 200HB generator. Heavy-atom soaks were performed in crystallization buffer lacking dithiothreitol and containing one of the following heavy-atom solutions: 0.6 mM $HgCl_2$ for 3 h, 0.8 mM thimerosal for 4 h, 2.5 mM uranyl acetate for 2 d. Molecular replacement and MIR analysis. The structure was determined by a combination of molecular replacement (MR) and multiple isomorphous replacement (MIR) methods. The positions of cyclin A and Cdk2 were determined by MR with the program AMORE[32], using the structure of the unphosphorylated binary complex[22]. The correlation coefficient was 0.59 for 10–4-Å data. Maps calculated from the MR solution had clear electron density for the LFG motif (Fig. 1) and the 3_{10} helix of p27. To obtain phases with reduced model bias, an MIR analysis was undertaken using heavy-atom sites identified with difference Patterson and model-phased difference Fourier methods. The MIR analysis with the CCP4 program suite[33] included anomalous scattering from the $HgCl_2$ and thimerosal derivatives and had a mean figure of merit of 0.56 for 20.0–3.2-Å data (nonisomorphism limited the use of derivative data to low resolution). Maps calculated from phases generated by combination of MIR and model phases showed continuous electron density for p27, with detailed features of p27 electron density becoming evident in α_{calc} maps upon further refinement. The structure was refined by simulated annealing with the program X-PLOR[34], using the free-R as a monitor of model quality (the final free-*R* was 26.9 for 7.0–2.3-Å data), followed by least-squares refinement with the program TNT[35]. The final model consists of residues 13–298 of Cdk2, residues 175–432 of cyclin A, residues 25–93 of p27, one phosphothreonine, one sulphate ion and 197 water molecules. A comparison with the structure of the phosphorylated cyclin A–Cdk2 complex[23] shows that cyclin A does not undergo any significant conformational changes. $R_{sym} = \Sigma_n\Sigma_i|I_{h,i} - I_h|/\Sigma_n\Sigma_i I_{h,i}$ for the intensity (I) of i observations of reflection h; mean isomorphous difference $= \Sigma|F_{PH} - F_P|/\Sigma F_{PH}$, where F_{PH} and F_P are the derivative and native structure factors, respectively; phasing power $= [(F^2_{H(calc)}/(F_{PH(obs)} - F_{PH(calc)})^2]^{1/2}$; *R* factor $= \Sigma|F_{obs} - F_{calc}|/\Sigma|F_{obs}|$, where F_{obs} and F_{calc} are the observed and calculated structure factors, respectively.

* Root-mean-square deviations from ideal geometry and root-mean-square variation in the B-factors of bonded atoms.

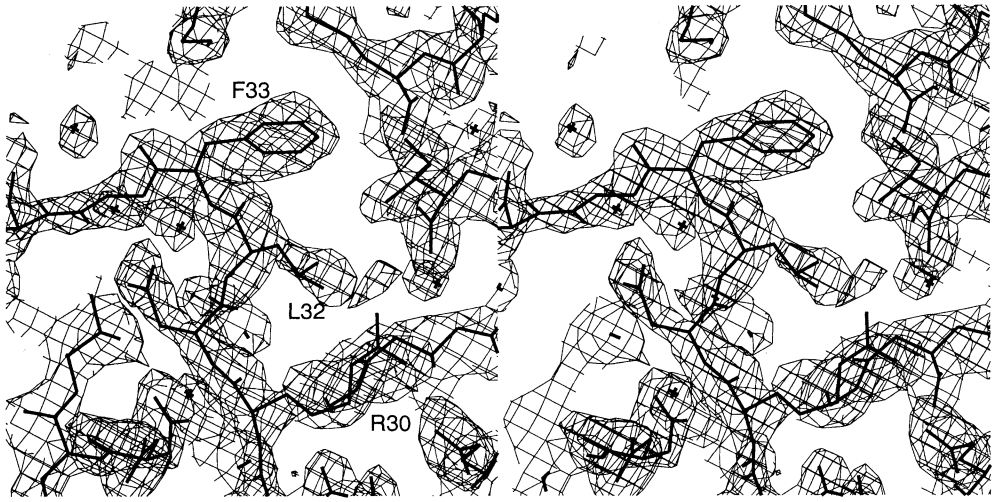

FIG. 1 Initial electron density of the LFG motif at the p27–cyclin A interface contoured at 1.0σ. The $(2|F_{obs}| - |F_{calc}|)$ Fourier synthesis was calculated at 2.3 Å resolution using phases derived from the cyclin A–Cdk2 molecular replacement model before any p27 was built into the model. Arg 30, Leu 32 and Phe 33 of p27 are labelled.

First, by rearranging the N-terminal β-sheet and the catalytic cleft, p27 would destabilize any ATP binding. Second, p27 fills up the catalytic cleft mimicking ATP, and eliminates any possibility of ATP binding. Third, p27 binds a peptide-binding groove of cyclin A, which is likely to be the docking site of a number of tight-binding substrates, also reducing the possibility that substrates may compete away the changes in the catalytic cleft of Cdk2.

p27–cyclin A interactions

The p27–cyclin A interactions are likely to be as important for binding as the p27–Cdk2 interactions because they account for 40% of the surface area buried, they include 35% of the short-distance hydrogen bonds, and they involve residues highly conserved among both the cyclin and p27 families. The most striking p27–cyclin A interactions involve the LFG coil binding a shallow groove of cyclin A consisting of the α1, α3 and α4 helices of the cyclin-box repeat (Fig. 3). The coil has a rigid conformation and low temperature factors in the crystals, due, in part, to intramolecular hydrogen bonds, in addition to cyclin A contacts. At its N terminus, the coil starts with a reverse turn (residues 26 to 29), followed by a short extended region (residues 29 to 31), and ending with another turn (residues 31 to 34) stabilized by an intramolecular side-chain–backbone hydrogen bond (Fig. 3*a*). The first turn and the extended region bind cyclin A primarily through hydrogen bonds, making 1 backbone–backbone, 3 side-chain–backbone and 3 side-chain–side-chain hydrogen bonds (see Fig. 3*a* and legend for a list). These interactions are augmented by van der Waals contacts made by Ala 28 to residues from the α1 and α4 helices.

The second turn contains the Leu 32 and Phe 33 residues of the

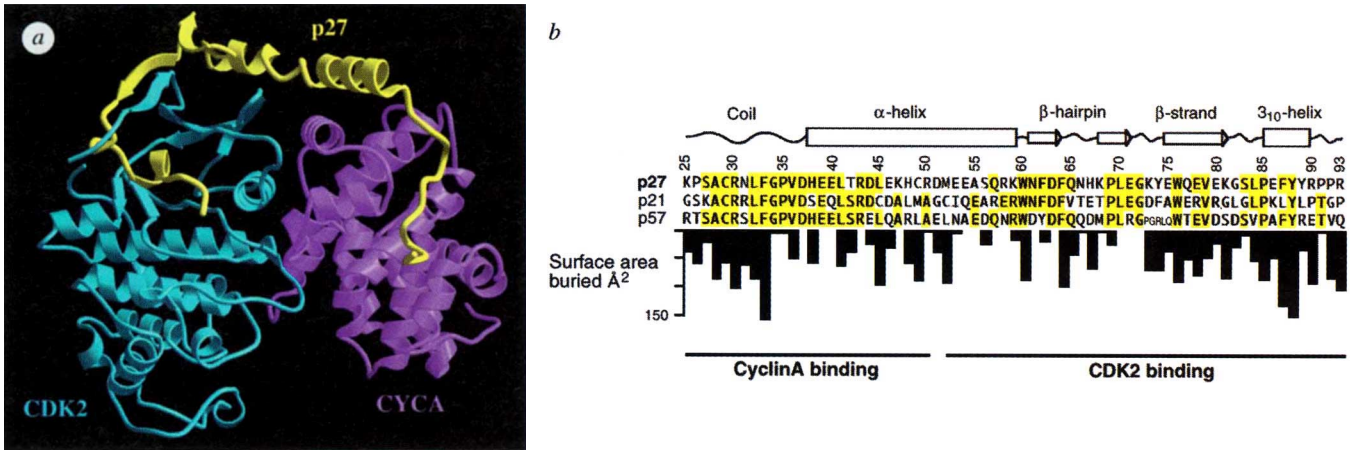

FIG. 2 *a*, p27 binds as an extended structure interacting with both cyclin A and Cdk2. Schematic drawing shows p27 in yellow, cyclin A in purple, and Cdk2 in cyan. The figure was prepared with the programs MOLSCRIPT[36] and RASTER3D[37]. *b*, Sequence of the p27 inhibitory domain showing its secondary structure elements and the homology with the corresponding domains of the p21 and p57 Kip/Cip family members (p21 starts at residue 14, and p57 at residue 26). Residues identical in two or more family members are highlighted in yellow. The bar graph shows the buried surface area per p27 amino acid upon complex formation. The structure of unbound p27 is not known, so for the surface accessibility calculations it was assumed to have the same structure as in the complex.

LFG motif, which bind deeper inside the cyclin A groove (Fig. 3*b*). This area of the cyclin A groove is lined with hydrophobic amino acids highly conserved among cyclins A, B, D1 and E (Met 210, Ile 213, Leu 214, Trp 217 of the α1 helix, and Leu 253, Arg 250 and Gln 254 of the α3 helix), and these amino acids make multiple van der Waals contacts to the Leu-Phe pair of p27 (Fig. 3*b*). The contacts to the α1 helix are particularly significant because the cyclin A residues involved are among the most highly conserved in the cyclin box (in bold: **MRAILVDW**).

The glycine of the LFG motif (Gly 34) has backbone ϕ–ψ angles that other amino acids cannot adopt, and in conjunction with the following proline (Pro 35), plays an important role in allowing the polypeptide chain to exit the cyclin A groove. After its exit from the groove, an amphipathic helix (His 38, Leu 41, Leu 45 and Cys 49 form the hydrophobic face of the helix) guides the chain towards Cdk2, in the process making a few additional van der Waals contacts with the α5 helix on the surface of cyclin A.

p27–Cdk2 interactions

These interactions involve the N-terminal lobe of Cdk2, which in the binary cyclin A–Cdk2 complex[22] contains a five-stranded β-sheet, as well as the catalytic cleft of Cdk2 occurring at the interface of the N- and C-terminal lobes. p27 uses three consecutive secondary structure elements, its β-hairpin, β-strand and 3_{10} helix, to clamp around the β-sheet of Cdk2 (Fig. 2). These three regions of p27 are likely to bind in a highly interdependent and cooperative fashion, because they rely on structural changes in CDK2 which they together induce.

First, the β-hairpin (residues 61–71), which is amphipathic, forms a sandwich with the N-terminal β-sheet of Cdk2, burying a large number of hydrophobic and aromatic amino acids both from p27 and Cdk2 (Fig. 4*a*, *b*). In this region of p27, the interacting amino acids include Trp 60, Phe 62, Phe 64, Pro 69, Tyr 74 and Trp 76, and they are highly conserved in the Kip/Cip family (Fig. 2*b*). On Cdk2, the interacting amino acids include Tyr 19, Ala 21, Val 30, Leu 32, Leu 67, Ile 70, Tyr 77 and Val 79, and they are generally conserved as hydrophobic amino acids in the Cdk family. In the binary cyclin A–Cdk2 complex, these hydrophobic Cdk2 amino acids instead pack against each other, their interactions being facilitated by the β-sheet being highly curved and partly folded upon itself (Fig. 4*c*). On p27 binding, the β-sheet flattens and exposes the hydrophobic amino acids to p27. In addition to the van der Waals contacts, this region of the interface also includes two backbone–side-chain hydrogen bonds, and two side-chain–side-chain hydrogen bonds (Fig. 4*a* legend).

The second portion of the p27–Cdk2 interface involves the p27 β-strand (residues 75–81) being incorporated into the Cdk2 β-sheet through six backbone–backbone β-sheet hydrogen bonds (with residues 16–22 of Cdk2 in an antiparallel arrangement). To accommodate the p27 strand, the first β-strand of Cdk2 (residues 1–13) is displaced and becomes disordered (Fig. 4*a*, *b*). This results in a p27–Cdk2 hybrid β-sheet that has four strands from Cdk2 and one strand from p27.

The third portion of the p27–Cdk2 interface involves the 3_{10} helix of p27 (residues 85–90) that binds deep inside the catalytic cleft and occupies most of the available space in the cleft (Fig. 5*a*). The helix axis is parallel with the long dimension of the cleft, and the helix traces the position that the ATP occupies in the binary complex[22,23]. In this region, the most significant contacts are made by Tyr 88, which is conserved in the Kip/Cip family (Fig. 2*b*). Its aromatic ring makes van der Waals contacts to Phe 80, Phe 82 and Leu 134 of Cdk2, and its hydroxyl group makes two hydrogen bonds to the backbone carbonyl of Glu 81 and the backbone amide of Leu 83 (Fig. 5*a*). The position of the tyrosine side chain in the catalytic cleft, and the Cdk2 contacts it makes, mimic those that are made by the purine base of ATP in the binary complex (Fig. 5*b*; ref. 22). In particular, the tyrosine hydroxyl group hydrogen bonds are analogous to the hydrogen bonds made by the N1 and N6 groups of the adenine base (Fig. 5*b*).

Other packing interactions in this region involve Phe 87, which is also positioned deep inside the catalytic cleft, making van der Waals contacts to Phe 80, Leu 134 and Ala 144 of Cdk2 (Fig. 5*a*).

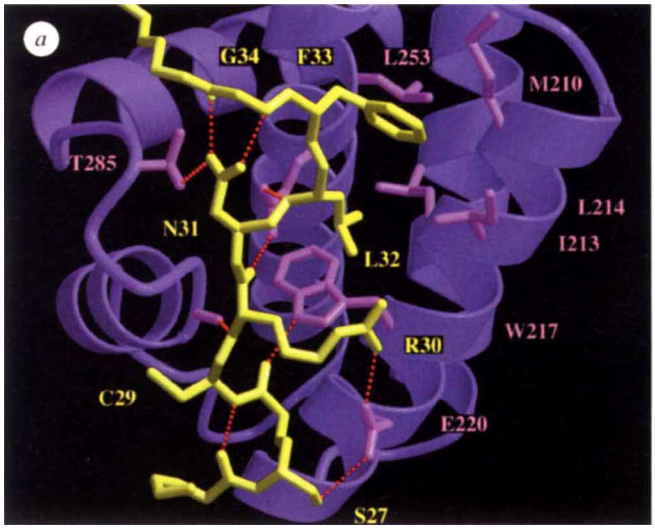

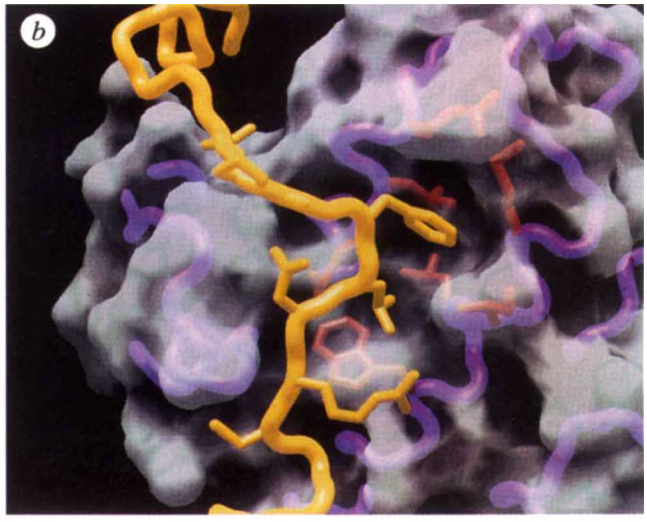

FIG. 3 *a*, The rigid coil of p27 binds a shallow cyclin A groove. View highlights the multiple hydrogen-bond (red dotted lines) and van der Waals contacts at the interface. The orientation and colouring are similar to those of Fig. 2*a*, except that side chains are coloured in a brighter tone than the backbone representations. On p27, side chains for residues 27–34 are shown, except for Ala 28 whose side chain points into the plane of the figure and is obstructed in this view; on cyclin A, only the interacting side chains are shown. Following is a complete list of intermolecular hydrogen bonds in this region: Ser 27 Oγ of p27 hydrogen bonds with Glu 220 Oε2 of cyclin A, Ala 28 carbonyl with Trp 217 Nε1, Arg 30 amide with Ile 281 carbonyl, Arg 30 Nη1 with Glu 220 Oε1, Arg 30 carbonyl with Gln 254 Nε2, Asn 31 Nδ2 with Thr 285 Oγ1, and Leu 32 amide with Gln 254 Oε1. *b*, Surface representation of cyclin A, highlighting the concave parts of the surface (in grey) that form the binding sites of the hydrophobic p27 amino acids in an orientation similar to that in *a*. Side chains shown in *a* are also shown here. The cyclin A surface was constructed with the program GRASP[38].

In addition to the van der Waals contacts, the 3_{10} helix also forms hydrogen bonds with conserved catalytic-site amino acids of Cdk2. The backbone carbonyl groups of Phe 87 and Arg 90 of p27 make hydrogen bonds to the conserved Lys 33 side chain of Cdk2. The positions of the Phe 87 and Arg 90 carbonyl groups are similar to those of the ATP phosphates in the binary complex, and the carbonyl–Lys 33 interactions mimic the ATP phosphate–Lys 33 interactions of the binary complex (Fig. 5*b*).

Structural changes in Cdk2

The five stranded β-sheet of Cdk2, which forms the roof of the catalytic cleft and plays a critical role in ATP binding[22], is altered by p27 binding in several ways. First, in the binary complex, the β-sheet is curved and partially folded upon itself burying a large number of hydrophobic amino acids (Fig. 4*c*). On p27 binding, the displacement of the first strand provides partial access to the hydrophobic patch by removing the Met 1 and Phe 4 side chains from the packing (Fig. 4*a*, *c*). The straight p27 strand that replaces it moves the N-terminal portion of the second Cdk2 strand by up to 8.5 Å, separating it partially from the rest of the β-sheet (Fig. 4*a*, *c*). These changes, along with the overall flattening of the β-sheet, are associated with the exposure of the hydrophobic patch and its repacking with the amphipathic p27 β-hairpin.

Second, in the binary complex, the loop between β-strands 1 and 2 (the glycine loop) folds partially over the ATP-binding portion of the cleft and binds the ATP phosphates[22,23]. On p27 binding, the glycine loop is eliminated, and the position that the glycine loop would occupy now has the coil immediately after the 3_{10} helix of p27. Furthermore, the partial separation of the second β-strand from the rest of the Cdk2 β-sheet also creates an opening in the roof of the catalytic cleft. These changes, which effectively open up the ATP-binding portion of the catalytic cleft, are accompanied by the binding of the p27 3_{10} helix, which is significantly bulkier than ATP, in the catalytic cleft.

The changes in the β-sheet, and in particular in the ATP-binding glycine loop, suggest that even in the absence of the 3_{10}

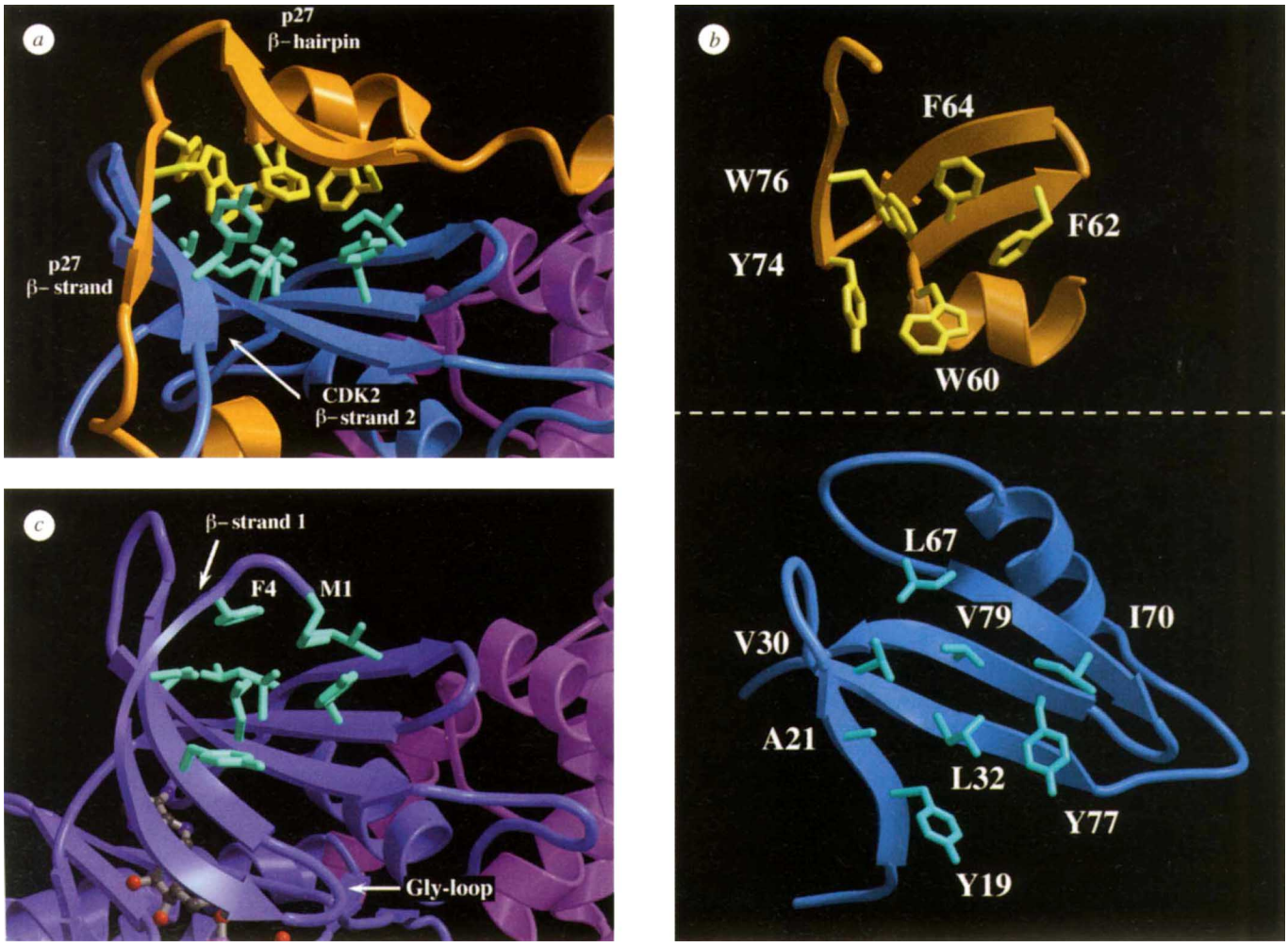

FIG. 4 *a*, The p27 β-hairpin forms a sandwich with the N-terminal β-sheet of Cdk2, resulting in changes in the structure of the N-terminal lobe of Cdk2. The orientation and colouring are similar to those of Fig. 2*a*. Additional contacts not mentioned in the text include hydrogen bonds from the Lys 75 side chain of Cdk2 to the backbone carbonyls of Phe 64 and Gln 65 of the β-hairpin tip, and hydrogen bonds from the Trp 60 and His 67 side chains of Cdk2 to the Asp 68 and Tyr 77 side chains of p27, respectively. *b*, The β-sandwich is opened up about the dotted line to show the hydrophobic amino acids, which are labelled. *c*, In the phosphorylated cyclin A–Cdk2 complex[22,23] the β-sheet is curved and partly folded upon itself, burying the hydrophobic amino acids which become exposed on p27 binding (Met 1, Phe 4, Tyr 19, Ala 21, Val 30, Leu 32, Leu 67, Ile 70, Tyr 77 and Val 79). The first strand of the β-sheet and the glycine-rich loop that folds over the ATP phosphates[22,23], are eliminated upon p27 binding. The Met1 and Phe4 residues are labelled; ATP is shown as a ball-and-stick representation.

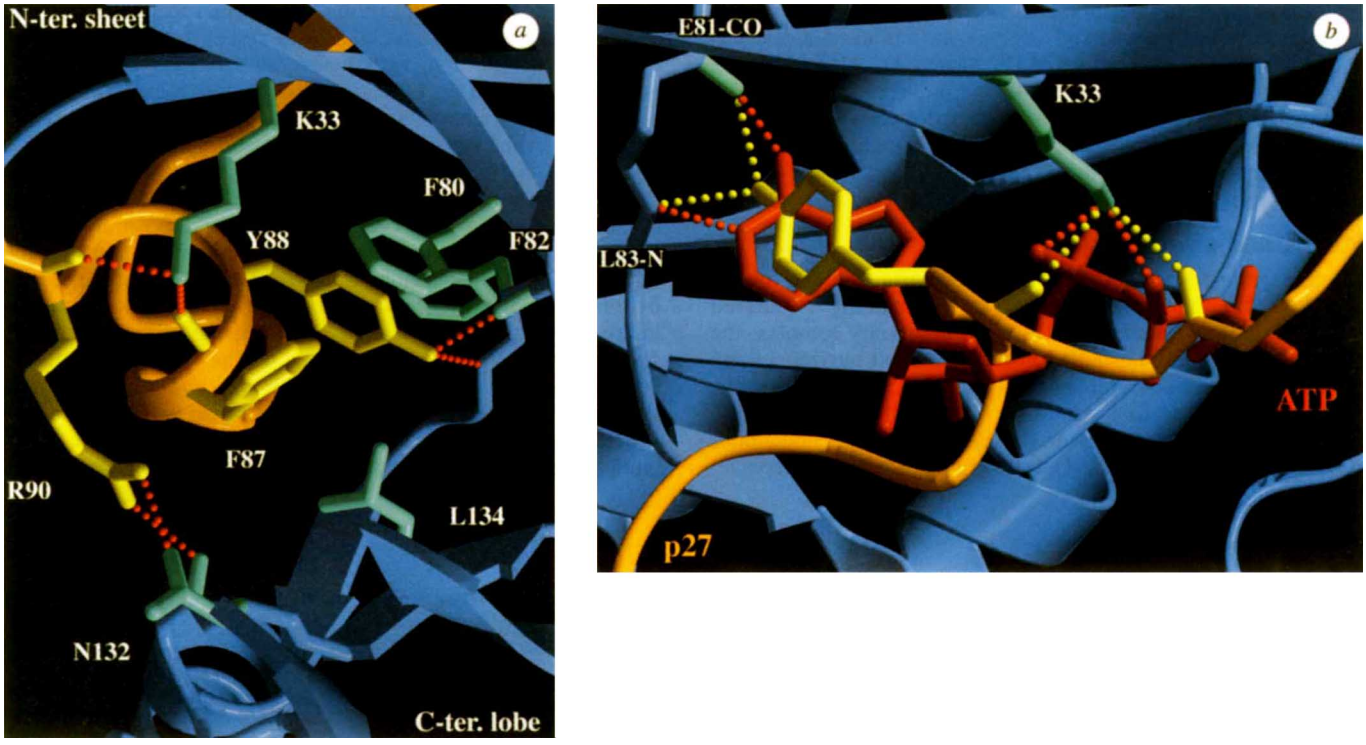

FIG. 5 *a*, The p27 3_{10} helix binds in the widened catalytic cleft of Cdk2 making multiple van der Waals and hydrogen-bond contacts (red dotted lines). View is rotated by roughly 90° about the vertical axis of Fig. 2*a*; colouring is as Fig. 2*a*. To make the contacts easier to see, parts of the N- and C-terminal lobes that would be above the plane of the figure are not shown. Hydrogen-bond contacts not mentioned in the text include ones by the Arg 90 side chain of p27 to the Asn 132 side chain and Gln 131 backbone carbonyl group of Cdk2. *b*, The p27 3_{10} helix mimics the ATP in the binary complex in its position and its Cdk2 contacts. Composite figure shows the ATP (red) from the phosphorylated binary complex[23] positioned by superimposing the Cdk2 molecules in the binary and tertiary complexes. The hydrogen bonds that ATP makes in the binary complex are indicated as red dotted lines and those made by p27 as yellow dotted lines. View is rotated by roughly 90° about the horizontal axis of Fig. 2*a*, so that the N-terminal β-sheet of Cdk2 is above the plane of the figure. The second strand of the β-sheet is not shown because it would obstruct this view of the catalytic cleft.

helix filling up the catalytic cleft, the kinase would have a reduced affinity for ATP. This is consistent with the observation that a truncated form of p27, lacking the 3_{10} helix residues, retains partial inhibitory activity[4,21].

Implications for Kip/Cip family function

The crystal structure of the p27–cyclin A–Cdk2 complex reveals that p27 has separate binding sites on the cyclin and CDK subunits and this explains how the Kip/Cip inhibitors can bind the isolated subunits. Binding to the cyclin–CDK complex is significantly tighter[12,18–20], consistent with cooperative binding to the two subunits.

LFG–cyclin A interactions. The LFG motif–cyclin interactions are likely to serve as an initial anchor in complex formation, because these interactions do not need structural rearrangements in cyclin to occur, in contrast to the Cdk2 interactions. The importance of the LFG–cyclin interactions is supported by the observation that a 25-amino-acid peptide encompassing the LFG motif of p21 can antagonize p21 binding to, and inhibition of, the cyclin–CDK complex[26].

The LFG–cyclin interactions involve conserved residues on both partners. The LFG motif corresponds to the region best conserved in the Kip/Cip family (Fig. 2*b*), and the region of cyclin A that forms the binding groove corresponds to the start of the cyclin box, also the region best conserved among cyclins A, B, D and E (ref. 22). This explains, in part, the specificity of the Kip/Cip proteins for complexes containing these cyclins. On the other hand, cyclin H (ref. 27) and p35 (ref. 8), which are CDK activators that do not bind the Kip/Cip inhibitors[28,29], are only distantly related to the cyclin-box cyclins, and do not have the p27-interacting amino acids conserved in the other cyclins. Cyclin H is a partner of Cdk7 in a CDK-activating kinase[27], and p35 is a partner of Cdk5 involved in neurite outgrowth[8,30], and their roles are consistent with their need to avoid inhibition by the Kip/Cip proteins.

The identification of a peptide-binding groove on cyclin A raises the possibility that other cyclin-interacting proteins may use peptide–groove interactions in their binding. Studies of the p107 CDK substrate have shown that it contains a sequence similar to the LFG motif that is necessary for its tight binding to the cyclin A–Cdk2 complex[25]. It is conceivable that variants of the LFG motif, perhaps not immediately recognizable from sequence alignment, may also be used by other proteins to bind the cyclin groove.

p27–Cdk2 interactions. The interactions with the cyclin may serve as an entry point for the Kip/Cip proteins into the cyclin–CDK complex, but the interactions with the CDK and the accompanying structural changes in the catalytic cleft are likely to be key determinants of inhibition. The inhibition constants (K_i) of the Kip/Cip inhibitors for different cyclin–CDK complexes vary considerably[20], even for complexes that have consensus residues in their cyclin grooves, and this modulation is likely to reside with the

CDK subunit. For example, the mitotic cyclin B–Cdc2 is only poorly inhibited by the Kip/Cip proteins[20], and this is probably due, in part, to a 35-amino-acid insertion at the N terminus of Cdc2. The insertion occurs within a region that corresponds to the first β-strand of Cdk2, and it is likely to interfere with the structural rearrangements in the N-terminal lobe that are necessary for CDK binding and inhibition. Furthermore, we note that the Cdk2 amino acids that make significant contacts to p27 are generally conserved in CDKs 4, 5 and 6, which are also targets of the Kip/Cip proteins, but not in Cdc2 (for example Lys 75 of Cdk2; Fig. 5*a* legend).

Kip/Cip binding to the cyclin–CDK complex also inhibits the phosphorylation of the CDK subunit by CAK[4,28,29], and this is probably a result of steric hindrance. In the crystal structure, which contains phosphorylated Cdk2 (ref. 23), the C terminus of the p27 inhibitory domain is within 8 Å of the phosphothreonine 160 on the T-loop of Cdk2, and a comparison with the unphosphorylated cyclin A–Cdk2 complex[22], which has a different T-loop conformation, suggests that p27 would be even closer to the unphosphorylated Thr 160. Full-length p27 contains an additional 105 residues following its inhibitory domain (p21 and p57 contain 82 and 220 additional residues, respectively), and we presume that a significant portion of these amino acids would be in the vicinity of the T-loop as the p27 chain exits the catalytic cleft of Cdk2 and may interfere with the binding of CAK to the T-loop.

Implications of two binding sites. The existence of two distinct binding sites on the cyclin–CDK complex could, in principle, allow the association of two inhibitor molecules with a single cyclin–CDK complex, one interacting with the cyclin, and the other with the CDK. However, this mode of binding will not be cooperative, and the equimolar complex should be greatly preferred. It has been proposed that there may be cyclin–CDK complexes associated with multiple inhibitor molecules[20,31]. In the case of cyclin A–Cdk2, we have not detected stable complexes containing multiple p27 molecules, even at high concentrations (up to 0.2 mM) and in the presence of excess p27 (Table 1). We surmise that in the case of cyclin A–Cdk2, two-inhibitor complexes are thermodynamically highly unfavoured over the equimolar complex, although their existence with other Kip/Cip–cyclin–CDK combinations remains a possibility.

The existence of two distinct binding sites could also allow, in principle, weak, unproductive association of a Kip/Cip inhibitor with a cyclin–CDK complex without significant inhibition of the catalytic activity[20,31]. Such a complex would require a cyclin that has a consensus LFG-motif binding site and a CDK subunit that is not susceptible to inhibitor binding, conditions that might theoretically be met by cyclin–CDK complexes other than cyclin A–Cdk2.

Conclusion

The inhibitory domain of p27 binds the cyclin A–Cdk2 complex as an extended structure interacting with both subunits. Key hydrophobic and hydrogen-bond interactions between a 10-amino-acid region of p27, which contains the conserved LFG sequence motif, and a shallow groove of cyclin A, which consists of conserved cyclin-box residues, are likely to serve as an anchor point in initial binding, facilitating subsequent interactions with Cdk2. p27 binding inhibits the CDK catalytic activity because its interactions with the N-terminal β-sheet of Cdk2 induce conformational changes that change the shape of the catalytic cleft and because p27 inserts into and fills up the catalytic cleft, eliminating any potential for ATP binding. □

Received 16 May; accepted 27 June 1996.

1. Pines, J. *Cancer Biol.* **6,** 63–72 (1995).
2. Peter, M. & Herskowitz, I. *Cell* **79,** 181–184 (1994).
3. Sherr, C. J. & Roberts, J. M. *Genes Dev.* **9,** 1149–1163 (1995).
4. Polyak, K. *et al. Cell* **78,** 59–66 (1994).
5. Reynisdóttir, I., Polyak, K., Iavarone, A. & Massagué, J. *Genes Dev.* **9,** 1831–1845 (1995).
6. Parker, S. B. *et al. Science* **267,** 1024–1027 (1995).
7. Liu, M., Lee, M. H., Cohen, M., Bommakanti, M. & Freedman, L. P. *Genes Dev.* **10,** 142–153 (1996).
8. Lee, M. H. *et al. Proc. natn. Acad. Sci. U.S.A.* **93,** 3259–3263 (1996).
9. El-Deiry, W. S. *et al. Cell* **75,** 817–825 (1993).
10. Soos, T. J. *et al. Cell Growth Differ.* **7,** 135–146 (1996).
11. Poon, R. Y. C., Toyoshima, H. & Hunter, T. *Molec. biol. Cell* **6,** 1197–1213 (1995).
12. Toyoshima, H. & Hunter, T. *Cell* **78,** 67–74 (1994).
13. Xiong, T. *et al. Nature* **366,** 701–704 (1993).
14. Gu, Y., Turck, C. W. & Morgan, D. O. *Nature* **366,** 707–710 (1993).
15. Harper, J. W., Adami, G. R., Wei, N., Keyomarsi, K. & Elledge, S. J. *Cell* **75,** 805–816 (1993).
16. Lee, M. H., Reynisdóttir, I. & Massagué, J. *Genes Dev.* **9,** 639–649 (1995).
17. Matsuoka, S. *et al. Genes Dev.* **9,** 650–662 (1995).
18. Chen, J., Jackson, P. K., Kirschner, M. W. & Dutta, A. *Nature* **374,** 386–388 (1995).
19. Lin, J., Reichner, C., Wu, X. & Levine, A. J. *Molec. cell. Biol.* **16,** 1786–1793 (1996).
20. Harper, J. W. *et al. Molec. Biol. Cell* **6,** 387–400 (1995).
21. Luo, Y., Hurwitz, J. & Massagué, J. *Nature* **375,** 159–161 (1995).
22. Jeffrey, P. D. *et al. Nature* **375,** 159–161 (1995).
23. Russo, A. R., Jeffrey, P. D. & Pavletich, N. P. *Nature struct. Biol.* (in the press).
24. Chothia, C. *J. molec. Biol.* **105,** 1–14 (1976).
25. Zhu, L., Harlow, E. & Dynlachtt, D. *Genes Dev.* **9,** 1740–1752 (1995).
26. Chen, I. *et al. Oncogene* **12,** 595–607 (1996).
27. Fisher, R. P. & Morgan, D. O. *Cell* **78,** 713–724 (1994).
28. Kato, J., Matsuoka, M., Polyak, K., Massagué, J. & Sherr, C. J. *Cell* **79,** 487–496 (1994).
29. Aprelikova, O., Xiong, Y. & Liu, E. T. *J. biol. Chem.* **270,** 18195–18197 (1995).
30. Nikolic, M., Dudek, H., Kwon, Y. T., Ramos, Y. K. & Tsai, L. H. *Genes Dev.* **10,** 816–825 (1996).
31. Zhang, H., Hannon, G. J. & Beach, D. *Genes Dev.* **8,** 1570–1758 (1994).
32. Navaza, J. *Acta Crystallogr.* A**50,** 157–163 (1994).
33. Collaborative Computational Project No. 4. *Acta Crystallogr.* D**50,** 760–763 (1994).
34. Brunger, A. T. *X-PLOR, a System for Crystallography and NMR* Version 3.0 Manual (Yale Univ. Press, New Haven, CT, 1991).
35. Tonrud, D. E., Ten Eyck, L. F. & Matthews, B. W. *Acta crystallogr.* A**43,** 489 (1987).
36. Kraulis, P. J. *J. appl. Crystallogr.* **24,** 946–950 (1991).
37. Merrit, E. A. & Murphy, M. E. *Acta crystallogr.* D**50,** 869–873 (1994).
38. Nicholls, A., Sharp, K. A. & Honig, B. *Proteins Struct. Funct. Genet.* **11,** 281–296 (1991).

ACKNOWLEDGEMENTS. A.A.R. and P.D.J. contributed equally to this work. We thank S. Geromanos of the Sloan-Kettering Microchemistry Facility for N-terminal sequence and mass spectroscopic analyses; K. Polyak for help with the inhibition assays; D. O. Morgan for providing us with the Cdk7 and cyclin H-expressing baculovirus vectors; and R. Kenny for administrative help. Supported by the NIH, the Pew Charitable Trusts, the Arnold and Mabel Beckman Foundation, the Dewitt Wallace Foundation, and the Samuel and May Rudin Foundation.

CORRESPONDENCE and requests for materials should be addressed to N.P.P. (e-mail: Nikola@xray2.mskcc.org). Coordinates have been deposited with the Brookhaven Protein Data Bank (ID code IJSU).